Experimental confirmation of the stability and chemical bonding analysis of the high-pressure phases Ca-I, II, and III at pressures up to 52 GPa

Q. F. Gu,[1] G. Krauss,[1] Yu. Grin,[2] and W. Steurer[1,*]
[1]*Department of Materials, Laboratory of Crystallography, ETH Zurich, CH-8093 Zurich, Switzerland*
[2]*Max-Planck-Institut für Chemische Physik fester Stoffe, D-01187 Dresden, Germany*
(Received 31 October 2008; published 30 April 2009)

Synchrotron x-ray powder diffraction on Ca was performed at pressures up to 52.6(3) GPa using a diamond-anvil cell at ambient temperature. The sequence of phase transitions from fcc (Ca-I) to bcc (Ca-II) at 19.8 GPa and bcc to simple cubic (sc Ca-III) at 33 GPa was confirmed. A sample of the Ca-III phase was remelted at a pressure above 40 GPa and still remained in the sc structure. The quality of the obtained powder diffraction patterns doubtlessly confirms the stability of the sc phase within the framework of the experiment at pressures above 33 GPa. The bulk modulus of the high-pressure phases was calculated based on fitting of third-order Birch-Murnaghan equations of state with $K=17.4(5)$ GPa, $K'=3.22(4)$ for fcc Ca-I, $K=51.9(3.4)$ GPa, $K'=4.2(6)$ for bcc Ca-II, and $K=165.2(4.7)$ GPa, $K'=1.0(3)$ for sc Ca-III, respectively. In terms of electron localizability indicator (ELI-D), the chemical bonding in the calcium modifications may be described as multicenter bonding. With increasing pressure, the number of centers per bond changes from 6 (and 4) in Ca-I via 4+2 for Ca-II to 8 for Ca-III.

DOI: 10.1103/PhysRevB.79.134121 PACS number(s): 61.66.Bi, 61.50.Ks, 31.10.+z, 62.50.−p

I. INTRODUCTION

Within the group of alkaline-earth metals, calcium takes a special position. Ca is the lightest element of the group, for which the energies of the *d* orbitals are close enough for being occupied by *s* electrons, i.e., a possible $4s \rightarrow 3d$ transfer. This property could explain its high-pressure structural chemistry[1] as well as the electrical properties of the high-pressure phases. Ca was found to be superconducting with a T_c up to 25 K at 161 GPa, which is the highest T_c found for an element up to now.[2] Its high-pressure structural chemistry is entirely different from that of the light alkaline-earth metals Be and Mg, which is dominated by $s \rightarrow p$ transfer. These metals form close-packed structures below 50 GPa. Mg transforms to a bcc phase at approximately 50 GPa. The heavier alkaline-earth metals Sr and Ba are characterized by a variety of high-pressure phases including modulated host-guest structures (see, e.g., McMahon and Nelmes,[3] and references therein). In contrast to these, Ca was reported to follow the simple sequence fcc (Ca-I), bcc (Ca-II), α-Po [simple-cubic (sc) Ca-III] with transition pressures of about 20 and 32 GPa.[1,4] This sequence implies that the coordination number decreases from 12 to 8 and to 6 with increasing pressure. This is inasmuch remarkable, as the sc phase was reported to be stable over a very wide pressure range between 32 and 113 GPa.[4] Furthermore, the occurrence of the sc phase is remarkable itself, as only a few elements, i.e., Po at ambient conditions, P at pressures above aproximately 10 GPa and As above approximately 25 GPa crystallize with this structure type.[3] In an earlier study, a possible transition into an unknown phase already at 42 GPa (Ref. 1) was reported.

There are several theoretical studies on Ca-I, II, and III high-pressure phases present to the literature,[5–8] but still discrepancies between calculation results and experiments exist, e.g., different transition pressures (9 GPa for fcc→bcc and 40 GPa for bcc→sc from calculation[7] compared to 20 and 32 GPa from experiments). Ahuja *et al.*[6] confirmed the sc structure as well as the wide pressure range of its existence theoretically, but also predicted sc phases for Na (above 140 GPa) and Mg (above 660 GPa), which were not confirmed experimentally at pressures up to 155 GPa for Na. Recent calculations on the sc phase of Ca indicate large imaginary phonon frequencies in the pressure range of 40–110 GPa, which imply a structural instability of the sc phase.[8] Very recently, also Ca-IV and Ca-V were subject of several theoretical and experimental studies, showing that no modulated structure was found for these two phases.[9–11]

The interest in the high-pressure crystal chemistry and the partly controversial results from theory and experiment were the motivation to reinvestigate the high-pressure behavior of Ca with the focus on the pressure range up to approximately 50 GPa. Due to the theoretically predicted instability of Ca-III, special emphasis was drawn on the quality of the obtained data and the experimentally determinable equilibrium phases. Chemical bonding analysis may help to understand the transition sequence.

II. EXPERIMENTAL

A. X-ray diffraction

High pressures up to 52.6(3) GPa were generated by the use of an ETH-type diamond-anvil cell (DAC) at ambient temperature. Degassed silicone oil (DMS-T31, polydimethylsiloxane, trimethylsiloxy terminated, viscosity 1000 cSt from ABCR) served as pressure-transmitting medium. All the sample manipulation on the high-purity calcium (4N, Alfa Aesar) was done in an argon-filled glove box. Preindented W gaskets with a typical thickness of 60 μm and a hole diameter of 125 μm were used. To minimize the deviatoric stress, the sample chamber was loaded with only a small slice of Ca with typically about $30\times30\times20$ μm^3 in size and filled with the pressure medium. A ruby crystal was

placed next to the Ca sample and the pressures were determined using the ruby fluorescence technique. With the used sample and gasket dimensions, no bridging of the Ca sample between the two diamond culets was observed up to the highest applied pressures. Synchrotron x-ray diffraction experiments were performed at ID27, ESRF, Grenoble, France and Materials Science (MS) beamline, Swiss Light Source (SLS) at Paul-Scherrer Institut (PSI), Villigen, Switzerland. Two-dimensional (2D) diffraction data were collected on a Marresearch charge-coupled device (CCD) (ID27) and mar345 image-plate detector (MS beamline) using a wavelength of 0.3738 Å and 0.5610 Å, respectively. The 2D diffraction images were integrated by the use of the program FIT2D (Ref. 12) and the one-dimensional (1D) powder pattern were refined by applying the Rietveld method using the program GSAS.[13,14] Equations of state were calculated by the use of the program EOSFIT5.2.[15]

B. Calculation procedure

Electronic structure calculations and bonding analysis were carried out using the TB-LMTO-ASA program package.[16] The Barth-Hedin exchange potential[17] was employed for the local-density approximation (LDA) calculations. The radial scalar-relativistic Dirac equation was solved to get the partial waves. The calculation within the atomic sphere approximation (ASA) includes corrections for the neglect of interstitial regions and partial waves of higher order.[18] Nevertheless, due to the special feature of the crystal structure, an addition of empty sphere E was necessary for Ca-III. The following radii of the atomic spheres were applied for the calculations for Ca-I $r(\mathrm{Ca})=2.184-1.837$ Å depending on the pressure (lattice parameter); for Ca-II $r(\mathrm{Ca})=1.734$ Å; and for Ca-III $r(\mathrm{Ca})=1.539$ Å, $r(\mathrm{E})=0.813$ Å. A basis set containing Ca($4s$,$4p$,$3d$) orbitals was employed for a self-consistent calculation with Ca($4f$) functions being downfolded. The electron localizability indicator (ELI, Y) (Ref. 19) was evaluated in the ELI-D representation according to Refs. 20 and 21 with an ELI module within the TB-LMTO-ASA (Ref. 16) program packages. ELI-D and electron density were analyzed using the program BASIN (Ref. 22) with consecutive integration of the electron density in basins, which are bound by zero-flux surfaces in the ELI-D or electron-density gradient field. Such treatment of ELI-D is similar to the procedure proposed by Bader[23] for the electron density.

III. RESULTS AND DISCUSSION

A. Structural studies

As Ca is very soft, special care has to be taken for the sample preparation. For this study, only a small amount of sample compared to the size of the sample chamber was used in order to avoid a bridging of the sample between the two diamond anvils what will cause a uniaxial pressure regime. The sharp ruby fluorescence signals indicated quasihydrostatic conditions within the whole framework of the experiments.

X-ray diffraction patterns were collected up to 52.6(3) GPa using small pressure steps. In accordance with experimental reports in the literature,[1,4] three different phases were observed within the investigated pressure range. The fcc phase was found to be stable up to 19.8 GPa. It transforms into the bcc phase, which transforms into the simple-cubic phase at approximately 33 GPa. Interestingly, no two-phase regions were observed within the framework of the experiments, indicating no kinetic hindering of the reconstructive phase transitions. Typical *in situ* x-ray diffraction patterns of the three different phases are shown in Fig. 1. The experimental lattice parameters were obtained by Rietveld refinements of the collected patterns. The lattice parameters as a function of pressure and the normalized volumes are listed in Table I. To compare the volume of the different phases, the values were normalized based on the calculated density of each phase. The normalized volume drops at the phase transitions which are about 3.1% (fcc→bcc) and 9.8% (bcc→sc), respectively. The observed transition pressures are comparable to the literature data;[1,4] the volume drops are slightly larger (2%–3% for fcc→bcc and 8% for bcc→sc, respectively[1,4]). A possible reason for this could be the nonhydrostatic conditions used in the experiments described in the literature. Similar to Yabuuchi *et al.*,[4] no additional phase transition at 42 GPa was observed as reported by Olijnyk and Holzapfel.[1] It has to be highlighted that the quality of the data, i.e., the absence of gasket reflections, allows the unambiguous determination of the structure type, as no reflections could be overlayed by the gasket reflections. Additional effects, e.g., strong preferred orientation can also be ruled out.

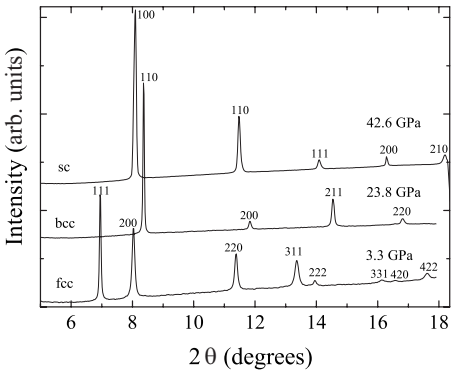

FIG. 1. Powder-diffraction pattern of the three stable high-pressure phases of Ca (ID27, $\lambda=0.3738$ Å).

In order to study the stability of the simple-cubic phase, one sample at a pressure of about 40 GPa was treated with a Nd:YAG laser operating at 28.3 W to remelt, recrystallize, and equilibrate the sample. Unfortunately, it was not possible to measure the sample temperature during the heat treatment process, but a different shape of the sample before and after the heat treatment indicated a melting and a recrystallization of the sample. No reaction between the pressure medium and the calcium sample was observed by the light microscopy as well as x-ray diffraction. After heat treatment, the sample still had the simple cubic structure. As the sample was remelted under pressure, it can be assumed that no preferred orientation induced by nonhydrostatic pressure conditions is present, which could strongly weaken additional sample reflections. A second sample was held at about 49 GPa and ambient temperature for 1 month. After this time, the sample

TABLE I. Observed lattice parameters (a) and normalized volume (V/V_0) of Ca as a function of pressure.

fcc			bcc			sc		
P/GPa	a/Å	V/V_0	P/GPa	a/Å	V/V_0	P/GPa	a/Å	V/V_0
1×10^{-4}	5.608(1)	1.0	19.9(1)	3.691(1)	0.57	33.8(4)	2.689(1)	0.441
2.5(1)	5.387(1)	0.886	21.0(3)	3.671(1)	0.561	38.2(5)	2.665(1)	0.429
3.3(2)	5.325(1)	0.856	23.8(2)	3.617(1)	0.536	42.6(3)	2.642(1)	0.418
3.7(1)	5.294(1)	0.841	24.4(1)	3.604(1)	0.530	46.0(4)	2.626(1)	0.410
5.5(2)	5.193(1)	0.794	25.3(2)	3.591(1)	0.525	51.6(2)	2.597(1)	0.397
7.5(1)	5.098(1)	0.751	27.4(1)	3.554(1)	0.509	52.6(3)	2.592(1)	0.395
9.5(1)	5.014(1)	0.715	29.9(1)	3.522(1)	0.495			
9.8(1)	5.011(1)	0.713	32.3(6)	3.495(1)	0.484			
11.7(2)	4.939(1)	0.683						
13.4(1)	4.877(1)	0.658						
13.7(1)	4.872(1)	0.656						
16.0(2)	4.802(1)	0.628						
16.4(1)	4.791(1)	0.624						
19.8(2)	4.698(1)	0.588						

was still single phase and contained only the simple cubic phase. After pressure release to ambient, calcium recovered in all experiments immediately to the fcc structure. The present experiments strongly indicate that the simple cubic phase is the stable equilibrium phase at pressures above 33 GPa and ambient temperature. This result is in contrast to a recent calculation of a phonon instability of the simple cubic structure,[8] which indicates a metastable structure. One reason for the discrepancies of calculation and experiment could be the fact that the calculations were done at a temperature of 0 K, which does not represent the experimental conditions. Our findings agree well with the theoretical work of Ahuja *et al.*[6] The transition pressure from the bcc to the sc phase are similar, whereas the pressure for the fcc to bcc transition is slightly higher (19.9 GPa instead of 15 GPa from calculations).

The compressibility of the high-pressure phases was calculated by fitting third-order Birch-Murnaghan equations of state to the volume as a function of pressure. The obtained values for the bulk modulus K and its pressure derivative K' are given in Table II and illustrated in Fig. 2. The fcc Ca-I is very soft and its compressibility comparable to argon, which is illustrated by a large volume drop of more than 40% from ambient pressure to the first phase transition at 19.8 GPa. The bulk modulus of Ca-II [$K=51.9(3.4)$ GPa] and Ca-III [$K=165.2(4.7)$ GPa] increases to higher values, as could be expected. With increasing pressure, the atomic volume decreases and Ca becomes stiffer. The interatomic distances decrease from 3.966 Å at 10^{-4} GPa (fcc) to 3.322 Å at 19.8 GPa (fcc) and 3.078 Å at 27.4 GPa (bcc), to 2.592 Å at 52.6 GPa (sc).

TABLE II. Bulk moduli K and their pressure derivatives K' for the three investigated high-pressure phases of Ca.

Phase	K (GPa)	K'
fcc	17.4(5)	3.22(4)
bcc	51.9(3.4)	4.2(6)
sc	165.2(4.7)	1.0(3)

B. Chemical bonding analysis

Application of high pressure influences immediately the electron density in the different modifications of calcium.

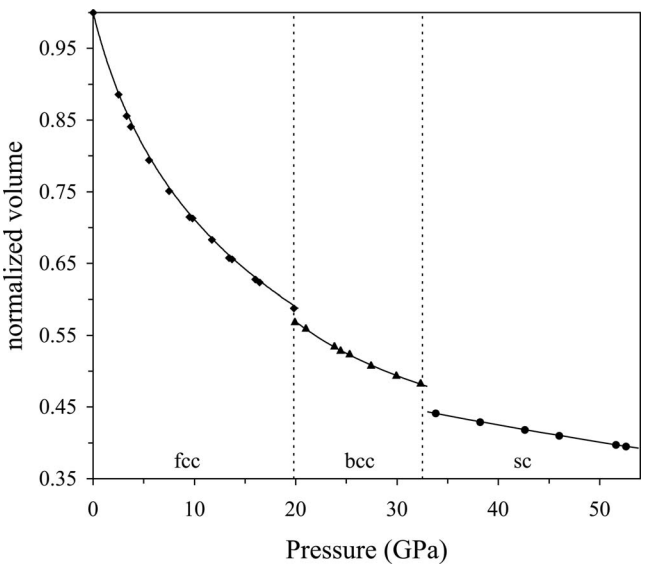

FIG. 2. Normalized volume of the investigated high-pressure phases of calcium as a function of pressure. The lines indicate the best fits of third-order Birch-Murnaghan equations of state. The errors are smaller than the size of the symbols.

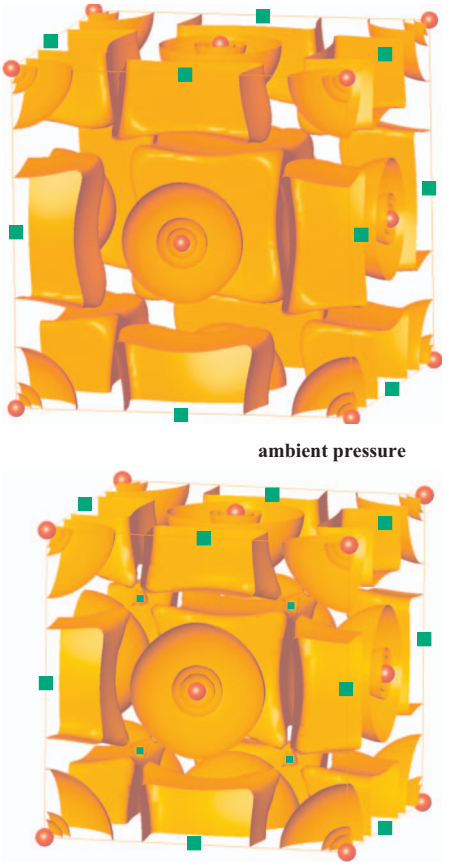

FIG. 3. (Color) Electron localizability indicator in Ca-I: (top) isosurface of ELI-D with Y=1.260 for the ambient pressure (a =5.608 Å); (bottom) isosurface of ELI-D with Y=1.136 for P =16.4 GPa (a=4.791 Å). Positions of the ELI-D attractors in the octahedral holes (6c bonds) are shown by large green rectangles; those in the tetrahedral holes (4c bonds) are shown by small green rectangles.

The topology of the electron density was used for the analysis of the chemical bonding within the quantum theory of atoms in molecules (QTAIMs).[23] Further development of the quantum chemical tools for bonding analysis in the real space resulted in the formulation of the ELI.[19] In the variant called ELI-D, the electron localizability information is obtained in the form of the product of the electron density (one-electron property) and pair-volume function (two-electron property). ELI-D depicts in real space the average charge in a (very small) microcell containing the same for all cells (fixed) fraction of same-spin electron pair. It allows both the analysis of the chemical bonding (based on the topology of ELI-D) in the sense of the two-electron behavior in real space, and, if necessary, an analysis of the orbital contributions to the ELI-D topology (one-electron behavior). Being a bridge between the orbital and the direct-space representation of chemical bonds, ELI-D is a very useful tool for the study of the chemical bonding in molecules and solids.[21,24] Recently, it was applied for the analysis of the bonding in the hexagonal closest-packed metals.[25] Thus it was logical to employ ELI-D also for the bonding analysis in the calcium modifications.

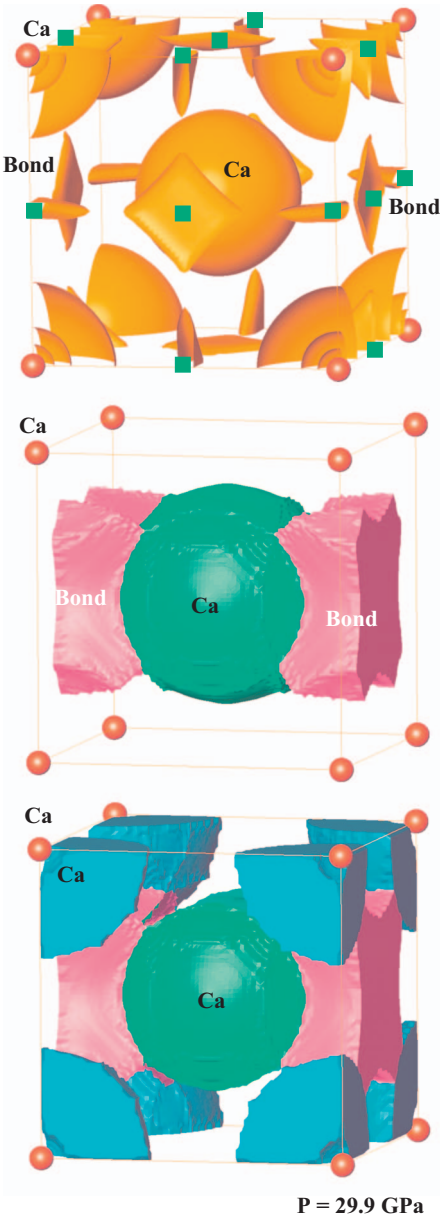

FIG. 4. (Color) Electron localizability indicator in Ca-II at 29.9 GPa (a=3.522 Å): (top) isosurface of ELI-D with Y=1.333 visualizing the positions of the bonding attractors in the octahedral holes (dark green rectangles); (middle) basins of the bonding attractor (violet) and calcium core attractor (green) having the largest contact surface to the bonding basin; (bottom) basin of the bonding attractor (violet) with complete environment of the core attractors (green and blue).

The distribution of ELI-D in fcc Ca-I at ambient pressure reveals only maxima in octahedral holes (Fig. 3, top). This picture remains independent on the pressure in the whole stability region of Ca-I. Only at the maximum pressure of 16.4 GPa additional attractors appear in the tetrahedral holes (Fig. 3, bottom). The total distribution reflects the multicenter bonding in the Ca-I modification (6c bonds in octahedral and 4c bonds in tetrahedral holes). Appearing of the bonding attractors in different holes of the fcc structural motif seems to be dependent on the calculation method.

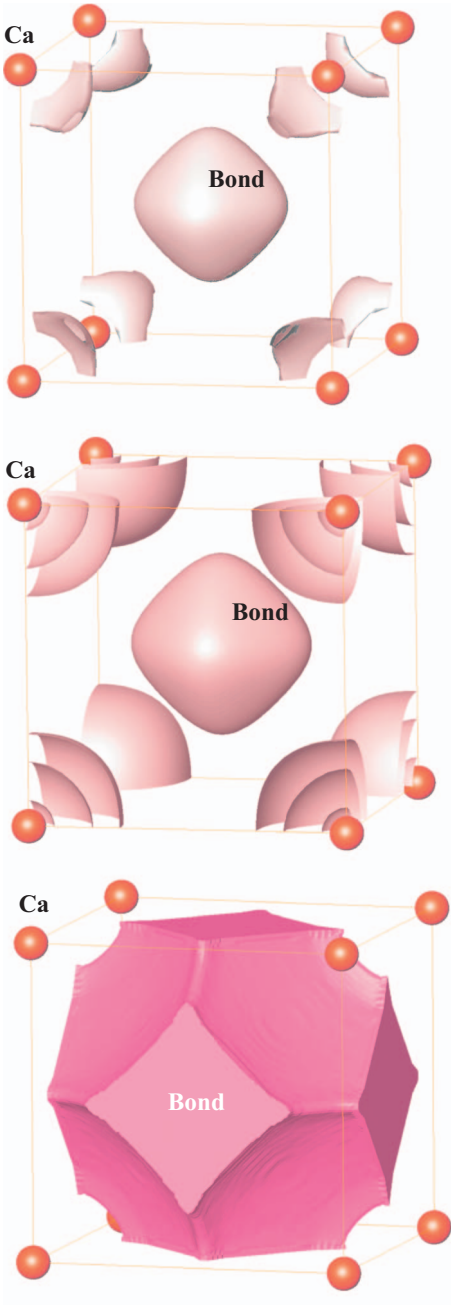

FIG. 5. (Color) Electron localizability indicator in Ca-III at 51.6 GPa (a=2.597 Å): (top) isosurface of ELI-D with Υ=1.845 visualizing the position of the bonding attractor and structuring (see "holes" in the surface along [100]) of the third shell of Ca; (middle) isosurface of ELI-D with Υ=1.650 illustrating the closing of the "holes" in the third shell; (bottom) basin of the bonding attractor (violet) with eight contact surfaces to the core attractors (convex hexagons).

Hartree-Fock (HF) calculations for Ca-I reveal electron localization function (ELF) maxima only in the tetrahedral holes.[26] For another fcc metal (Cu), the picture is a reverse one: whereas the HF calculation shows 6c and 4c bonds, the LMTO-ASA and FPLO calculations reveal only 4c bonds with the attractors in the tetrahedral holes.[27] The inner (third) shell of Ca keeps mainly the spherical distribution of ELI-D characteristic for the isolated atom. This is quantified by a low value of the structuring index (the difference between the highest ELI-D value in the examined shell and the ELI-D value at which the localization domain is without a "hole"[16]). The respective index for Ca-I is ε_{Ca}=0.04–0.07 with a weak increase tendency depending on the pressure, suggesting that the electrons of the third shell are not participating in the bonding within the valence region even at relatively high pressure up to 19.8 GPa. The ELI-D distribution in Ca-II is typical for the bcc structural motif. The attractors appear not on the shortest Ca-Ca contacts along [111] but in the octahedral holes on the second long Ca-Ca bonds along [100] (Fig. 4, top). The basin of the bonding attractor contacts six neighboring core basins indicating 6c bonds. A more close view reveals that each bonding basin has two large and four smaller contact surfaces to the Ca cores, allowing a more precise 2c+4c description (Fig. 4, middle and bottom). The structuring index for the third shell is still low (ε_{Ca}=0.06), characterizing a rather "passive" behavior of these electrons in the bonding.

The ELI-D distribution in Ca-III has two striking features: the bonding attractor at $\frac{1}{2},\frac{1}{2},\frac{1}{2}$ and the strongly structured third shell (Fig. 5). The basin of the bonding attractor has eight equivalent contact surfaces to the core regions, thus reflecting 8c bonding (Fig. 5, bottom). The maximal ELI-D value in the third shell is 1.885; the "holes" are completely closed at Υ=1.773 yielding the value of ε_{Ca}=0.112 which is double as large as in both other modifications. This is a fingerprint of the participation of the third shell in the bonding interaction.[24,28] At this point, it is not clear how far this feature of ELI-D is reflecting an s-d transformation possible for s elements at high pressures.[29]

IV. CONCLUSION

The structure of Ca was studied as a function of pressure up to 52.6(3) GPa. In accordance with the experimental reports in the literature, two first-order phase transitions were observed. Ca transforms at 19.8 GPa from the fcc to the bcc and at 33 GPa from the bcc to the simple-cubic type. The sequence of phase transitions was confirmed. The quality of the data and the results on annealing of Ca-III clearly indicate that this is the stable phase in the pressure range above 33 GPa at ambient temperature. In terms of ELI-D, the chemical bonding in the investigated modifications can be described as the multicenter bonding. ELI-D reveals the participation of the third shell in the bonding interaction in Ca-III but not in Ca-I and in Ca-II.

ACKNOWLEDGMENTS

Part of this work was performed at the Swiss Light Source, Paul Scherrer Institut, Villigen, Switzerland. Experimental assistance from the staff of the MS-Beamline at SLS, PSI, Villigen and ID27 at ESRF, Grenoble is gratefully acknowledged. We thank R. J. Angel for helpful comments on the use of EOSFIT5.2 and the Swiss National Science Foundation (SNF) for financial support under Contract No. 200021-115871.

*walter.steurer@mat.ethz.ch

[1] H. Olijnyk and W. B. Holzapfel, Phys. Lett. **100A**, 191 (1984).
[2] T. Yabuuchi, T. Matsuoka, Y. Nakamoto, and K. Shimizu, J. Phys. Soc. Jpn. **75**, 083703 (2006).
[3] M. I. McMahon and R. J. Nelmes, Chem. Soc. Rev. **35**, 943 (2006).
[4] T. Yabuuchi, Y. Nakamoto, K. Shimizu, and Y. Kikegawa, J. Phys. Soc. Jpn. **74**, 2391 (2005).
[5] J. W. McCaffrey, J. R. Anderson, and D. A. Papacanstantopoulos, Phys. Rev. B **7**, 674 (1973).
[6] R. Ahuja, O. Eriksson, J. M. Wills, and B. Johansson, Phys. Rev. Lett. **75**, 3473 (1995).
[7] F. Jona and P. M. Marcus, J. Phys.: Condens. Matter **18**, 4623 (2006).
[8] G. Gao, Y. Xie, T. Cui, Y. Ma, L. Zhang, and G. Zou, Solid State Commun. **146**, 181 (2008).
[9] H. Fujihisa, Y. Nakamoto, K. Shimizu, T. Yabuuchi, and Y. Gotoh, Phys. Rev. Lett. **101**, 095503 (2008).
[10] Y. Yao, J. S. Tse, Z. Song, D. D. Klug, J. Sun, and Y. Le Page, Phys. Rev. B **78**, 054506 (2008).
[11] T. Ishikawa, A. Ichikawa, H. Nagara, M. Geshi, K. Kusakabe, and N. Suzuki, Phys. Rev. B **77**, 020101(R) (2008).
[12] A. P. Hammersley, S. O. Svensson, M. Hanfland, A. N. Fitch, and D. Hausermann, High Press. Res. **14**, 235 (1996).
[13] A. C. Larson and R. B. Von Dreele, Los Alamos National Laboratory Report No. 86, 2000 (unpublished).
[14] B. H. Toby, J. Appl. Crystallogr. **34**, 210 (2001).
[15] R. J. Angel, Rev. Mineral. Geochem. **41**, 35 (2000).
[16] O. Jepsen, A. Burkhardt, and O. K. Andersen, The Program TB-LMTO-ASA, version 4.7 (Max-Planck-Institut für Festkörperforschung, Stuttgart, 1999).
[17] U. von Barth and L. Hedin, J. Phys. C **5**, 1629 (1972).
[18] O. K. Andersen, Phys. Rev. B **12**, 3060 (1975).
[19] M. Kohout, Int. J. Quantum Chem. **97**, 651 (2004).
[20] M. Kohout, F. R. Wagner, and Y. Grin, Int. J. Quantum Chem. **106**, 1499 (2006).
[21] M. Kohout, Faraday Discuss. **135**, 43 (2007).
[22] M. Kohout, BASIN, version 4.4 (Max-Planck-Institut für Chemische Physik fester Stoffe, Dresden, 2008).
[23] R. F. W. Bader, *Atoms in Molecules: A Quantum Theory* (Oxford University Press, Oxford, 1999).
[24] F. R. Wagner, V. Bezugly, M. Kohout, and Y. Grin, Chem.-Eur. J. **13**, 5724 (2007).
[25] A. I. Baranov and N. Kohout, J. Comput. Chem. **29**, 2161 (2008).
[26] B. Silvi and K. Gatti, J. Phys. Chem. A **104**, 947 (2000).
[27] A. Ormeci, H. Rosner, F. R. Wagner, M. Kohout, and Y. Grin, J. Phys. Chem. A **110**, 1100 (2006).
[28] M. Kohout, F. R. Wagner, and Y. Grin, Theor. Chem. Acc. **108**, 150 (2002).
[29] U. Schwarz, Z. Kristallogr. **219**, 376 (2004), and references therein.